REPORT

QUANTUM DEVICES

Coherent manipulation of an Andreev spin qubit

M. Hays[1]*, V. Fatemi[1]*, D. Bouman[2,3], J. Cerrillo[4,5], S. Diamond[1], K. Serniak[1]†, T. Connolly[1], P. Krogstrup[6], J. Nygård[6], A. Levy Yeyati[5,7], A. Geresdi[2,3,8], M. H. Devoret[1]*

Two promising architectures for solid-state quantum information processing are based on electron spins electrostatically confined in semiconductor quantum dots and the collective electrodynamic modes of superconducting circuits. Superconducting electrodynamic qubits involve macroscopic numbers of electrons and offer the advantage of larger coupling, whereas semiconductor spin qubits involve individual electrons trapped in microscopic volumes but are more difficult to link. We combined beneficial aspects of both platforms in the Andreev spin qubit: the spin degree of freedom of an electronic quasiparticle trapped in the supercurrent-carrying Andreev levels of a Josephson semiconductor nanowire. We performed coherent spin manipulation by combining single-shot circuit–quantum-electrodynamics readout and spin-flipping Raman transitions and found a spin-flip time T_S = 17 microseconds and a spin coherence time T_{2E} = 52 nanoseconds. These results herald a regime of supercurrent-mediated coherent spin-photon coupling at the single-quantum level.

A weak link between two superconductors hosts discrete, fermionic modes known as Andreev levels (*1*). These levels govern the physics of the weak link on the microscopic scale, ultimately giving rise to macroscopic phenomena such as the Josephson supercurrent. Superconducting electrodynamic qubits rely on the nonlinearity of the supercurrent in Josephson tunnel junctions, a manifestation of the ground-state properties of millions of Andreev levels acting in concert (*2*). Although the vast majority of conduction electrons undergo collective nonlinear bosonic oscillations in the superconducting condensate, each Andreev level can be occupied by a fermionic electronic excitation known as a Bogoliubov quasiparticle.

It was proposed that quantum information could be stored in the spin of a quasiparticle trapped in a weak link possessing a spin-orbit interaction (*3*). This Andreev spin qubit (ASQ) would carry a spin-dependent supercurrent, opening paths for spin manipulation and measurement unavailable to electrostatically confined spin qubits (*4*–*7*). In particular, this supercurrent could provide strong coupling between the spin and a superconducting microwave resonator (*8*–*13*). In the context of such supercurrent-based integration of Andreev levels with circuit quantum electrodynamics (cQED), pairs of quasiparticles have been coherently generated and recombined (*14*, *15*). However, because Andreev levels in most weak links are paired into spin-degenerate doublets, quasiparticle spin manipulation has remained elusive.

Weak links composed of superconductor-proximitized semiconductor nanowires ("Josephson nanowires" for short) offer a platform to investigate spinful Andreev physics (*16*–*18*). The Andreev spectra of Josephson nanowires was recently observed, owing to the development of an atomically perfect superconductor-semiconductor interface. This in turn revealed a rich interplay between superconductivity, spin-orbit interaction, electromagnetic field effects, and device geometry. Properties of Andreev levels in superconductor-semiconductor nanowires have been exploited to realize gate-tunable weak links for superconducting qubits (*19*, *20*), probe non-abelian Andreev levels known as Majorana zero modes (*21*), and relevant to this experiment, investigate spin-split doublets without a Zeeman field (*18*, *22*).

We performed coherent manipulation of the spin of an individual quasiparticle excitation of a superconductor. A naturally occurring quasiparticle is stochastically trapped in the Andreev levels of a Josephson nanowire (*14*, *15*), where it then resides predominantly in the

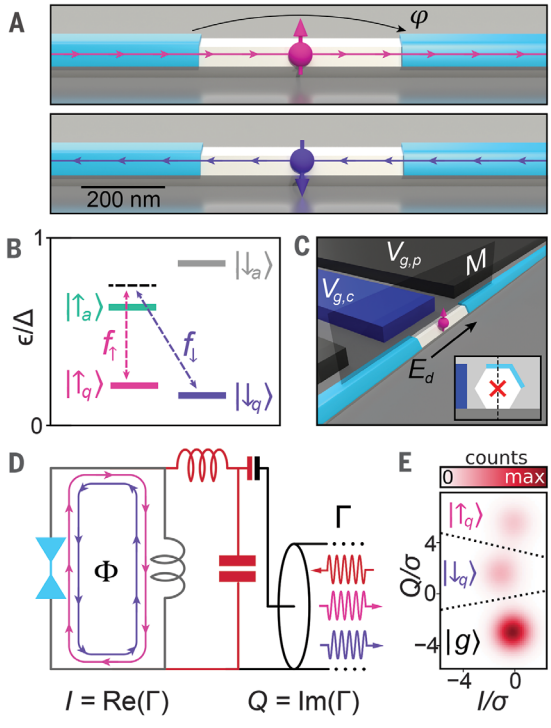

Fig. 1. Principle of the ASQ. (**A**) Illustration of a semiconductor nanowire (white) coated with epitaxial superconducting leads (light blue). The pair potential Δ of the leads confines the quasiparticle to the weak link. Because of spin-orbit interaction, if the quasiparticle is in the spin-up state (top), supercurrent flows to the right near zero phase bias φ = 0, whereas in the spin-down state (bottom), supercurrent flows to the left. Nonzero φ thus breaks spin degeneracy. (**B**) Energies of two Andreev doublets tuned to a Λ configuration. Two microwave drives (frequencies $f_\uparrow$, $f_\downarrow$) are equally detuned from $|\uparrow_q\rangle \leftrightarrow |\uparrow_a\rangle$ and $|\downarrow_q\rangle \leftrightarrow |\uparrow_a\rangle$, inducing a Raman process between the qubit states $|\uparrow_q\rangle$ and $|\downarrow_q\rangle$ by way of a virtual level (black dashed line). (**C**) Both drives induce an rf electric field E_d between the superconducting leads. But for a nanowire symmetric across the plane *M* (only nanowire + substrate), drive-induced spin-flips would be forbidden. (Inset) However, the mirror symmetry is broken by both the partial aluminum shell as well as the cutter (blue, bias $V_{g,c}$) and plunger gates (black, bias $V_{g,p}$). (**D**) The Josephson nanowire (light blue) is embedded in a superconducting loop (gray), which enables phase bias through an external flux $\varphi \approx 2\pi\Phi/\Phi_0$ as well as inductive coupling to a superconducting microwave resonator (dark red). The resonator reflection coefficient $\Gamma = I + iQ$ is probed with a tone near its fundamental frequency f_r = 9.188 GHz. (**E**) Histogram of repeated 1.9-μs measurements of Γ clustered into three distributions, corresponding to $|\uparrow_q\rangle$, $|\downarrow_q\rangle$, and $|g\rangle$ (standard deviation σ). The system state was assigned according to thresholds indicated with the black dotted lines.

[1]Department of Applied Physics, Yale University, New Haven, CT 06520, USA. [2]QuTech and Delft University of Technology, 2600 GA Delft, Netherlands. [3]Kavli Institute of Nanoscience, Delft University of Technology, 2600 GA Delft, Netherlands. [4]Área de Física Aplicada, Universidad Politécnica de Cartagena, E-30202 Cartagena, Spain. [5]Departamento de Física Teórica de la Materia Condensada C-V, Universidad Autónoma de Madrid, E-28049 Madrid, Spain. [6]Center for Quantum Devices, Niels Bohr Institute, University of Copenhagen, Universitetsparken 5, 2100 Copenhagen, Denmark. [7]Condensed Matter Physics Center (IFIMAC) and Instituto Nicolás Cabrera, Universidad Autónoma de Madrid, E-28049 Madrid, Spain. [8]Quantum Device Physics Laboratory, Department of Microtechnology and Nanoscience, Chalmers University of Technology, SE 41296 Gothenburg, Sweden.
***Corresponding author. Email: max.hays@yale.edu (M.H.); valla.fatemi@yale.edu (V.F.); michel.devoret@yale.edu (M.H.D.)**
†Present address: MIT Lincoln Laboratory, 244 Wood Street, Lexington, MA 02420, USA.

two spin states of the lowest-energy Andreev doublet with roughly equal probability (*22*). First, we initialized this ASQ by post-selecting on a single-shot cQED spin measurement (*22*). We then achieved coherent control of the ASQ by driving Raman transitions in a Λ system formed by the two spin states and an auxiliary higher-energy Andreev level. We observed spin lifetimes of up to T_S = 17 μs and a spin coherence time T_{2E} = 52 ns, which appears to be limited by a spinful bath.

Our realization of the ASQ hinges on the interplay between spin-orbit interaction in the semiconductor nanowire and the superconducting phase bias across the weak link (Fig. 1A) (*3*–*6*, *18*, *22*). In a conventional weak link, a trapped quasiparticle is restricted to spin-degenerate Andreev doublets, and therefore the spin cannot be coherently manipulated. In a Josephson nanowire, however, an intersubband spin-orbit interaction can cause spin to hybridize with translational degrees of freedom (this hybridized spin is sometimes known as pseudospin; we will continue to refer to it as "spin" for simplicity). Because of this interaction between spin and motion, the two spin states of an Andreev doublet carry equal and opposite supercurrent $\pm I_S/2$ at φ = 0, with I_S being doublet dependent (*5*). Then, because energy varies linearly with $\int Id\varphi$, the doublet degeneracy can be lifted with a nonzero phase bias: Perturbatively near φ = 0, the spin splitting is $\epsilon_s = I_S\varphi\Phi_0/2\pi$.

Microwave quantum optics techniques are well suited to achieve quasiparticle spin manipulation, given such a phase-induced spin splitting. In this experiment, the two spin states $|\downarrow_q\rangle, |\uparrow_q\rangle$ of one Andreev doublet form the qubit basis (Fig. 1B), while a second, higher-energy doublet provides auxiliary states $|\downarrow_a\rangle, |\uparrow_a\rangle$ critical for both qubit control and measurement (*22*). The number of Andreev doublets is given roughly by the ratio between the weak link length (here, ≈500 nm) and the superconducting coherence length (typically ~200 nm for the presented device parameters) (*5*, *6*, *18*). To manipulate the ASQ, we used the qubit states $|\downarrow_q\rangle, |\uparrow_q\rangle$ in conjunction with $|\uparrow_a\rangle$ as a Λ system. We applied simultaneous microwave drives to both the $|\uparrow_q\rangle \leftrightarrow |\uparrow_a\rangle$ transition (drive frequency $f_\uparrow$) and $|\downarrow_q\rangle \leftrightarrow |\uparrow_a\rangle$ (drive frequency $f_\downarrow$). By equally detuning the two drives from their respective transitions, a Raman process is induced so that the $\{|\downarrow_q\rangle, |\uparrow_q\rangle\}$ manifold can be coherently manipulated while $|\uparrow_a\rangle$ remains minimally populated.

The success of the Raman process is contingent on driving both the spin-conserving transition $|\uparrow_q\rangle \leftrightarrow |\uparrow_a\rangle$ and the spin-flipping transition $|\downarrow_q\rangle \leftrightarrow |\uparrow_a\rangle$. In principle, a radio frequency (rf) electric field can flip spin by coupling to the spatial character of the spin-orbit hybridized Andreev levels (*23*). However, as we outline here [(*24*), section 1], a broken spatial symmetry of the Josephson nanowire system is also required. Our hexagonal nanowire was made of [001] wurtzite indium arsenide grown by use of molecular beam epitaxy. Such a nanowire lying alone on a substrate would possess a transverse mirror symmetry (Fig. 1C); this property would then be inherited by the levels of the nanowire so that one spin state of each doublet would be mirror-symmetric and the other spin state mirror-antisymmetric (mirror character coincides with spin component character). Because we applied the drive voltage along the weak link, the rf electric field did not break the mirror symmetry—it points along the nanowire—and therefore would not flip spin.

In our device, the mirror symmetry is broken by both the superconducting leads and the electrostatic gates (Fig. 1C) as well as any symmetry-breaking disorder present in the nanowire. The superconducting leads consist of 10-nm-thick epitaxial aluminum, of which a 500-nm length was removed to form the weak link. The aluminum only covers two of six nanowire facets, breaking the mirror symmetry of the nanowire-substrate system. Because the gates are fabricated on one side of the nanowire, they also break the mirror symmetry. Both the cutter and plunger gates were used to tune the transparency of the weak link and were biased to $V_{g,c}$ = −71.9 mV and $V_{g,p}$ = 4.0 mV, respectively, unless otherwise noted [system tune up is provided in (*24*), section 2].

As mentioned above, the ASQ appears spontaneously when a quasiparticle is stochastically trapped in the Josephson nanowire. These nonequilibrium quasiparticles are ubiquitous in superconducting circuits and likely originate from background ionizing radiation and infrared photons (*25*, *26*). By embedding the Josephson nanowire in a cQED architecture (Fig. 1D), the effect of spin-orbit interaction can be harnessed to determine whether a trapped quasiparticle is in the "spin down" state $|\downarrow_q\rangle$ or the "spin up" state $|\uparrow_q\rangle$ or whether the weak link is in the ground state $|g\rangle$, where no quasiparticles are present (Fig. 1E) (*22*). For the bias conditions presented in this work, a quasiparticle remained trapped in the weak link on average 22 ± 1 μs and had a spin-flip lifetime T_S = 17 ± 1 μs [(*24*), section 6]. Below, we present data in terms of spin state occupation probabilities $P_\uparrow$, $P_\downarrow$ computed on the basis of the thresholds displayed in Fig. 1E. Because the two spin states were occupied with roughly equal probability, under any coherent manipulation $|\downarrow_q\rangle \leftrightarrow |\uparrow_q\rangle$ the observed spin state populations would not change. Throughout this work, we overcame this problem by preparing the quasiparticle in $|\uparrow_q\rangle$ by means of an initial readout pulse and post-selection [$|\downarrow_q\rangle$ post-selection is provided in (*24*)].

The first step in driving the Raman process (Fig. 1B) was to locate the two transitions that defined the Λ system: $|\uparrow_q\rangle \leftrightarrow |\uparrow_a\rangle$ and $|\downarrow_q\rangle \leftrightarrow |\uparrow_a\rangle$. After breaking spin degeneracy with Φ = −0.010Φ_0 (Fig. 1D), we measured the spectrum (Fig. 2A) using two-tone spectroscopy, without spin initialization. The dip in $P_\uparrow$ at 13.00 GHz corresponds to the drive coming into resonance with the $|\uparrow_q\rangle \leftrightarrow |\uparrow_a\rangle$ transition, resulting in population transfer out of $|\uparrow_q\rangle$ and into $|\uparrow_a\rangle$. Similarly, the dip in $P_\downarrow$ at 13.68 GHz corresponds to the $|\downarrow_q\rangle \leftrightarrow |\uparrow_a\rangle$ transition. Taking the difference yields the spin splitting ϵ/h = 680 MHz.

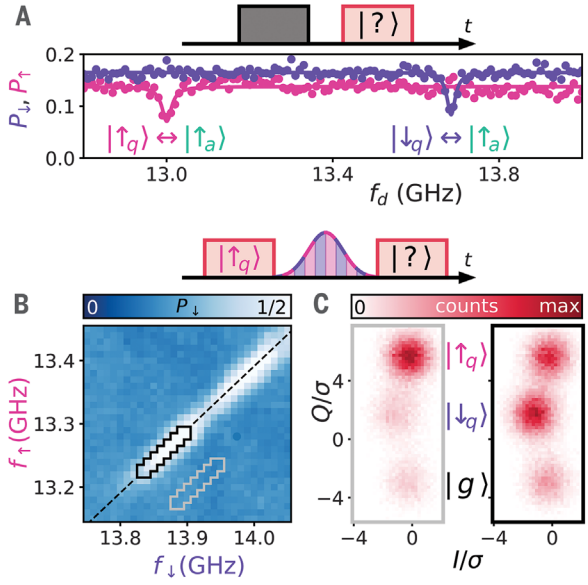

Fig. 2. Raman transitions of a trapped quasiparticle. (**A**) Two-tone spectroscopy of the $|\uparrow_q\rangle \leftrightarrow |\uparrow_a\rangle$ and $|\downarrow_q\rangle \leftrightarrow |\uparrow_a\rangle$ transitions consisting of a saturation pulse (gray, 1 μs long with variable carrier frequency f_d) followed by a readout pulse (dark red). (**B**) The quasiparticle was first prepared in $|\uparrow_q\rangle$ by means of an initial readout pulse and postselection. Simultaneous Gaussian pulses [235 ns full width at half maximum, 30 dB more power than used in (A)] with variable frequencies $f_\uparrow$, $f_\downarrow$ were then applied, followed by a final readout pulse. Color shows probability of measuring $|\downarrow_q\rangle$, and the peak in the final $|\downarrow_q\rangle$ population lies along $f_\downarrow = f_\uparrow$ = 610 MHz (black dashed line). (**C**) Full Γ histograms of the final readout pulse for the two subsets of measurements enclosed by the gray and black solid lines in (B). Data accrued in the region enclosed by the black line (right) show appreciable population transfer $|\uparrow_q\rangle \rightarrow |\downarrow_q\rangle$ compared with data enclosed by the gray line (left).

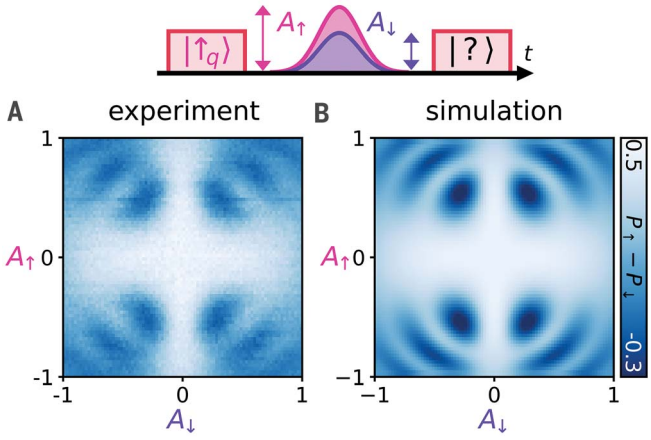

Fig. 3. Coherent Λ-Rabi oscillations of the ASQ. $f_\downarrow$ = 13.280 GHz; $f_\uparrow$ = 13.964 GHz. Color represents the probability difference between $|\uparrow_q\rangle$ and $|\downarrow_q\rangle$ after the drive. (**A**) Varying the amplitudes $A_\downarrow$, $A_\uparrow$ of the simultaneous drive pulses (94 ns full width at half maximum) resulted in oscillations between $|\uparrow_q\rangle$ and $|\downarrow_q\rangle$. (**B**) Simulated dynamics of the quasiparticle under the action of the drive pulses. The reduced contrast observed in (A) is taken into account by using the measured readout fidelities.

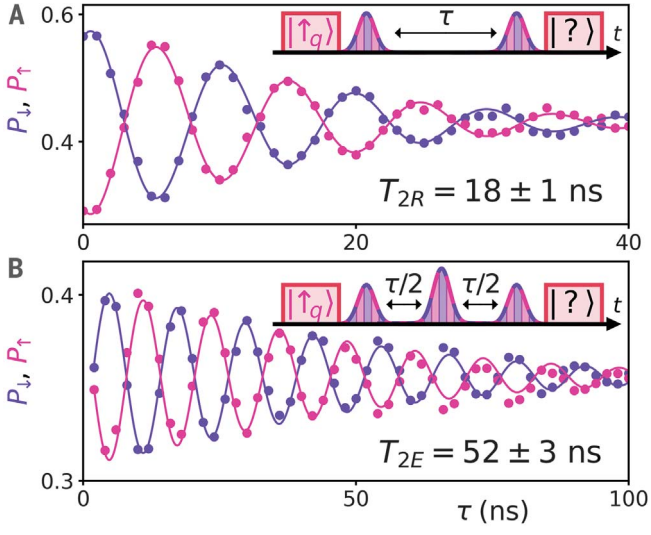

Fig. 4. Coherence decay of the ASQ. $V_{g,c}$ = −59.1 mV; $V_{g,p}$ = −33.3 mV; Φ = −0.115Φ_0. (**A**) Ramsey and (**B**) Hahn-echo experiments reveal T_{2R} = 18 ± 1 ns and T_{2E} = 52 ± 3 ns, respectively (supplemenatary materials, materials and methods). Oscillations were introduced in both cases by adding a phase proportional to τ to the final Raman pulse. The smaller value of $P_\uparrow + P_\downarrow$ in (B) as compared with (A) is likely due to additional quasiparticle detrapping $|\downarrow_q\rangle, |\uparrow_q\rangle \rightarrow |g\rangle$ caused by the echo pulse.

After initializing the quasiparticle in $|\uparrow_q\rangle$, we applied two simultaneous Gaussian pulses with variable respective carrier frequencies $f_\uparrow$ and $f_\downarrow$ and then measured the final state (Fig. 2B) [a wider frequency range is available in (*24*), section 3]. Along the line $f_\downarrow = f_\uparrow + 610$ MHz, we observed an increased $|\downarrow_q\rangle$ population that we attribute to a Raman process. As expected for Raman transitions, the slope of the line is unity because a shift of one drive frequency must be compensated by an equal shift of the other. The discrepancy between the spin splitting ϵ/h = 680 MHz and the 610 MHz offset is due to an uncontrolled jump of the Andreev spectrum that occurred between the measurements shown in Fig. 2, A and B (*24*).

We then proceeded to coherent manipulation of the spin of an individual quasiparticle. Parking $f_\uparrow$, $f_\downarrow$ on resonance with the Raman process [(*24*), section 4], we varied the amplitudes $A_\uparrow$, $A_\downarrow$ of the two Gaussian pulses before determining the final quasiparticle state (Fig. 3A). The observed oscillations in the spin population difference are characteristic of a coherent Raman process. Qualitatively, when either $A_\uparrow = 0$ or $A_\downarrow = 0$, there is no population transfer because both drives are required for the Raman process. As the amplitudes of both drives are increased (roughly along the diagonals $|A_\uparrow| \cong |A_\downarrow|$), the spin population difference undergoes coherent oscillations. As expected, the data are symmetric under $A_\uparrow \rightarrow -A_\uparrow$ and $A_\downarrow \rightarrow -A_\downarrow$. Quantitatively, we verified this interpretation by using a Lindblad master equation to numerically calculate the dynamics induced by the drive pulse (Fig. 3B) (*24*). We then fit the simulation to the measured data by varying the four interdoublet transition matrix elements, a slight detuning from the Raman resonance condition (fitted value 5.5 ± 0.1 MHz), and a phenomenological drive-induced detrapping rate (fitted value 10.8 ± 0.9 MHz at $|A_\uparrow| = |A_\downarrow| = 1$) to capture the measured increase of $|\downarrow_q\rangle, |\uparrow_q\rangle \rightarrow |g\rangle$ for larger drive powers.

We then characterized the coherence lifetime of an Andreev spin by performing Ramsey (Fig. 4A) and Hahn-echo experiments (Fig. 4B). The measured coherence times, T_{2R} = 18 ± 1 ns and T_{2E} = 52 ± 3 ns, are similar to what has been measured for spin-orbit qubits (*23*, *27*). However, we found that coherence lifetimes of so-called "pair transitions" were systematically an order of magnitude longer [(*24*), section 5]. In a pair transition, two quasiparticles are excited out of the condensate into both levels of a doublet so that the transition frequency is agnostic to baths that couple to spin (*14*, *15*, *18*). It therefore appears that the much shorter ASQ coherence lifetime is limited by such a spin-coupled bath—perhaps hyperfine interactions with the spinful nuclei of indium and arsenic [although nuclear baths typically have a lower frequency spectrum than the measured ratio $\frac{T_{2E}}{T_{2R}} = 2.9$ would indicate (*28*)], phonon-induced fluctuations of spin-orbit coupling, or paramagnetic impurities on the nanowire surface (*7*).

At the heart of the ASQ lies a spin-dependent supercurrent, presenting a natural mechanism for coherent integration of spins and electrodynamic modes at the single-quantum level. This fusion of superconducting electrodynamic qubits and semiconductor spin qubits has the potential to inherit the benefits of both platforms while leaving behind certain shortcomings. In modern many-qubit superconducting processors, the qubit size is comparable with that of the readout resonators (*29*). The ASQ presents the possibility to shrink the qubit area by a factor of more than a thousand without sacrificing coupling strengths. The small spatial footprint of the ASQ also protects it from dielectric loss mechanisms prevalent in superconducting qubits, and experiments following the path carved by electrostatically confined spins (such as the dynamics in tesla-scale magnetic fields) may diagnose the decoherence mechanisms observed here (*7*). The effects of dephasing and quasiparticle de-trapping could be mitigated by the use of a resonant stimulated Raman adiabatic passage (STIRAP) protocol, which would reduce the required pulse lengths and amplitudes (*30*). Last, our single-spin manipulation techniques could be used in conjunction with a superconducting bus to achieve gates between spatially distant spin qubits, a long-standing goal in the spin qubit community (*8*–*13*).

REFERENCES AND NOTES

1. I. Kulik, *J. Exp. Theor. Phys.* **30**, 944 (1969).
2. M. H. Devoret, R. J. Schoelkopf, *Science* **339**, 1169–1174 (2013).
3. N. M. Chtchelkatchev, Y. V. Nazarov, *Phys. Rev. Lett.* **90**, 226806 (2003).
4. C. Padurariu, Y. V. Nazarov, *Phys. Rev. B Condens. Matter Mater. Phys.* **81**, 144519 (2010).
5. A. A. Reynoso, G. Usaj, C. A. Balseiro, D. Feinberg, M. Avignon, *Phys. Rev. B Condens. Matter Mater. Phys.* **86**, 214519 (2012).
6. S. Park, A. L. Yeyati, *Phys. Rev. B* **96**, 125416 (2017).
7. R. Hanson, L. P. Kouwenhoven, J. R. Petta, S. Tarucha, L. M. K. Vandersypen, *Rev. Mod. Phys.* **79**, 1217–1265 (2007).
8. K. D. Petersson *et al.*, *Nature* **490**, 380–383 (2012).

9. N. Samkharadze *et al.*, *Science* **359**, 1123–1127 (2018).
10. X. Mi *et al.*, *Nature* **555**, 599–603 (2018).
11. T. Cubaynes *et al.*, *npj Quantum Inf.* **5**, 47 (2019).
12. F. Borjans, X. G. Croot, X. Mi, M. J. Gullans, J. R. Petta, *Nature* **577**, 195–198 (2020).
13. A. Wallraff *et al.*, *Nature* **431**, 162–167 (2004).
14. C. Janvier *et al.*, *Science* **349**, 1199–1202 (2015).
15. M. Hays *et al.*, *Phys. Rev. Lett.* **121**, 047001 (2018).
16. P. Krogstrup *et al.*, *Nat. Mater.* **14**, 400–406 (2015).
17. D. J. van Woerkom *et al.*, *Nat. Phys.* **13**, 876–881 (2017).
18. L. Tosi *et al.*, *Phys. Rev. X* **9**, 011010 (2019).
19. T. W. Larsen *et al.*, *Phys. Rev. Lett.* **115**, 127001 (2015).
20. G. de Lange *et al.*, *Phys. Rev. Lett.* **115**, 127002 (2015).
21. V. Mourik *et al.*, *Science* **336**, 1003–1007 (2012).
22. M. Hays *et al.*, *Nat. Phys.* **16**, 1103–1107 (2020).
23. S. Nadj-Perge, S. M. Frolov, E. P. Bakkers, L. P. Kouwenhoven, *Nature* **468**, 1084–1087 (2010).
24. Materials and methods are available as supplementary materials.
25. L. J. Swenson *et al.*, *Appl. Phys. Lett.* **96**, 263511 (2010).
26. M. Houzet, K. Serniak, G. Catelani, M. H. Devoret, L. I. Glazman, *Phys. Rev. Lett.* **123**, 107704 (2019).
27. J. W. van den Berg *et al.*, *Phys. Rev. Lett.* **110**, 066806 (2013).
28. F. K. Malinowski *et al.*, *Nat. Nanotechnol.* **12**, 16–20 (2017).
29. F. Arute *et al.*, *Nature* **574**, 505–510 (2019).
30. J. Cerrillo, M. Hays, V. Fatemi, A. Levy Yeyati, *Phys. Rev. Res.* **3**, 022012 (2020).

ACKNOWLEDGMENTS

We thank G. de Lange for assistance with device design and thank N. Frattini and V. Sivak for providing us with a superconducting nonlinear asymmetric inductive element (SNAIL) parametric amplifier. We are grateful to M. Goffman, C. Metzger, H. Pothier, L. Tosi, and C. Urbina for sharing their experimental results and hypotheses. We acknowledge useful discussions with N. Frattini, L. Frunzio, L. Glazman, M. Houzet, P. Kurilovich, V. Kurilovich, and C. Marcus. **Funding:** This research was supported by the US Army Research Office (ARO) grant W911NF-18-1-0212. M.H. acknowledges partial support from the ARO (W911NF-18-1-0020). S.D. acknowledges partial support from the ARO (W911NF-16-1-0349). The view and conclusions contained in this document are those of the authors and should not be interpreted as representing the official policies, either expressed or implied, of the ARO or the US government. The US government is authorized to reproduce and distribute reprints for government purposes notwithstanding any copyright notation herein. D.B. acknowledges support by the Netherlands Organisation for Scientific Research (NWO) and Microsoft Corporation Station Q. J.C. acknowledges the support from MICINN (Spain) ("Beatriz Galindo" Fellowship BEAGAL18/00081). J.N. acknowledges support from the Danish National Research Foundation. Some of the authors acknowledge the European Union's Horizon 2020 research and innovation program for financial support; A.G received funding from the European Research Council, grant 804988 (SiMS); and A.G., A.L.Y., J.C., and J.N. further acknowledge grant 828948 (AndQC) and QuantERA project 127900(SuperTOP). A.L.Y. acknowledges support by Spanish MICINN through grants FIS2017-84860-R and through the "María de Maeztu" Programme for Units of Excellence in R&D (grant MDM-2014-0377). **Author contributions:** M.H., V.F., K.S., D.B., T.C., A.G., and M.H.D. designed the experimental setup. P.K. and J.N. developed the nanowire materials. D.B. and A.G. fabricated the device. M.H. and V.F. performed the measurements. V.F., M.H., J.C., and A.L.Y. developed the symmetry analysis and microscopic modeling. M.H., J.C., V.F., and A.L.Y. developed and performed the Raman simulations. M.H., V.F., K.S., S.D., and M.H.D. analyzed the data. M.H., V.F., and M.H.D. wrote the manuscript, with feedback from all authors. **Competing interests:** The authors declare no competing interests. **Data and materials availability:** All data are available in the main text or supplementary materials.

SUPPLEMENTARY MATERIALS

science.sciencemag.org/content/373/6553/430/suppl/DC1
Supplementary Text
Figs. S1 to S9
Table S1
References (*31*–*37*)

17 January 2021; accepted 27 May 2021
10.1126/science.abf0345

Coherent manipulation of an Andreev spin qubit

M. Hays, V. Fatemi, D. Bouman, J. Cerrillo, S. Diamond, K. Serniak, T. Connolly, P. Krogstrup, J. Nygård, A. Levy Yeyati, A. Geresdi and M. H. Devoret

Science **373** (6553), 430-433.
DOI: 10.1126/science.abf0345

Superconducting spin qubit

To date, the most promising solid-state approaches for developing quantum information-processing systems have been based on the circulating supercurrents of superconducting circuits and manipulating the spin properties of electrons in semiconductor quantum dots. Hays *et al.* combined the desirable aspects of both approaches, the scalability of the superconducting circuits and the compact footprint of the quantum dots, to design and fabricate a superconducting spin qubit (see the Perspective by Wendin and Shumeiko). This so-called Andreev spin qubit provides the opportunity to develop a new quantum information processing platform.

Science, abf0345, this issue p. 430; see also abk0929, p. 390